IFSCC 2025 full paper (IFSCC2025-1154)

Virtual Screening of Botox-like Cosmetic Active Peptides Targeting the SNARE Complex and Syt1 C2B Domain

Rong Tang [1,*], Xichao Fu [1], Na Yang [1], Meijin Li [1], Yunpeng Dong [1], Dan Liu [1], Meng Wang [1], Zichen Liu [1], Xiaolin Tang [1] and Minhua Hong [1]

[1] Shanghai Peptide Biotechnology Co., Ltd, Shanghai, 201708, China

Abstract

Inhibition of the fusion between neurotransmitter-loaded synaptic vesicles and the presynaptic membrane to prevent the release of neurotransmitters (NT) such as acetylcholine (ACh) into the synaptic cleft may impede neuromuscular transmission at nerve terminals, thereby inducing facial muscle relaxation. This mechanism constitutes a potential therapeutic strategy against wrinkles. The SNARE complex, composed of three neuronal proteins—VAMP2, Syntaxin, and SNAP25—plays a pivotal role during the process of membrane fusion. The SNARE complex zippers in a directional manner from its membrane-distal N-terminal domains (NTDs) to its C-terminal domains (CTDs). The assembly of the NTDs serves as a critical and rate-limiting step in SNARE complex formation and membrane fusion. Recent experiments indicates that the interaction between the C2B domain of synaptotagmin 1 (Syt1) and the SNARE complex also performs as a key factor in Ca2+-dependent exocytosis and neurotransmitter release. Additionally, experimental evidence showed that certain botox-like peptides that function as SNARE modulators may inhibit Syt1, providing new ideas for the discovery of botox-like peptides.

This study describes a virtual screening approach. This approach integrates molecular docking, molecular dynamics (MD) simulations, and binding free energy calculations to conduct a simultaneous evaluation concerning the affinity of active peptides for the NTDs of the SNARE complex and the C2B domain of Syt1. Consequently, the screening identified several botox-like cosmetic active peptides capable of forming specific non-covalent interactions with both receptors, with MD simulations indicating that these complex systems remained stable throughout the simulation. Following the screening approach, three active peptides show promising botox-like peptides potential, with bioassay validation confirming that two of them effectively inhibit ACh release in neurons.This study provides a novel strategy for discovering botox-like cosmetic active peptides and offers potential candidate structures for further bioassay validation and active peptide development.

Key words: Botox-like peptides; Molecular docking; Molecular dynamics simulation; SNARE; Synaptotagmin

1. Introduction

A prominent manifestation of skin ageing is the formation of wrinkle, characterized by distinct depth and persistence in regions such as the forehead and periorbital areas. Dynamic facial expressions mediated by repetitive contractions of muscle fbres in the face contribute significantly to the formation of wrinkles. From a pathophysiological perspective, the mechanical traction exerted by hyperactive facial musculature induces inward displacement of cutaneous layers, thereby generating characteristic epidermal folding [1].

Current therapeutic strategies focus on neuromodulatory interventions targeting either direct myorelaxation through inhibition of efferent neural signaling or attenuation of neuromuscular transmission efficacy. This approach aims to reduce actin-myosin contractility, thereby diminishing mechanical stress on the dermoepidermal junction and mitigating wrinkle formation [2].

The primary therapeutic agents used are botulinum neurotoxins (BoNTs), which are potent biological substances originally identified as causative agents of botulism. When appropriately diluted, these neurotoxins have gained regulatory approval for clinical and aesthetic applications. Currently, localized injections of BoNT serotype A (BoNT/A) or B (BoNT/B) represent one of the most prevalent minimally invasive cosmetic procedures for facial rejuvenation and wrinkle reduction [3].

Botulinum neurotoxins (BoNTs) function as metalloproteases that potently inhibit Ca^{2+} -dependent neurotransmitter release by targeting critical components of synaptic vesicle fusion machinery. These enzymes specifically cleave three essential SNARE proteins: vesicle-associated membrane protein (VAMP) on synaptic vesicles (v-SNARE), synaptosome-associated protein 25 (SNAP-25) and syntaxin-1 (Syn) on the plasma membrane (t-SNARE). Through proteolytic disruption of these proteins, BoNTs destabilize the SNARE complex formation required for synaptic vesicle docking and fusion with presynaptic membranes. This molecular interference effectively blocks Ca^{2+}-triggered exocytosis, preventing acetylcholine release at neuromuscular junctions [4].

Substantial clinical evidence indicates that localized BoNT injections can induce both direct and indirect effects on non-target tissues, with severe cases potentially resulting in muscle paralysis [5].

These safety limitations underscore the imperative to develop and validate non-toxic molecular analogs that replicate BoNTA's therapeutic mechanisms. A prime example is Argireline (Ac-EEMQRR-NH2), a synthetic peptide clinically proven to exhibit Botox-like activity by modulating SNARE complex dynamics [1, 4].

The SNARE complex—VAMP2, syntaxin-1 and SNAP25—forms a parallel four-helix bundle essential for Ca^{2+}-triggered acetylcholine release at neuromuscular junctions. Structural analyses reveal that VAMP2 on synaptic vesicles zippers with syntaxin-1 and SNAP25 on the presynaptic membrane, creating a coiled-coil structure that forces membrane apposition. The energy released during SNARE zippering drives vesicle docking and fusion by overcoming repulsive forces between lipid bilayers, ultimately forming a fusion pore [6–8].

The zippering of SNARE complexes occurs through sequential N-terminal (NTDs) and C-terminal (CTD) assembly phases. NTDs interactions between v- and t-SNAREs induce a critical conformational shift that preorganizes the t-SNARE's CTD into a four-helix bundle configuration, templating the binding interface for subsequent CTD engagement. Biophysical evidence shows NTDs assembly exhibits slower kinetics (K_D ~10 μM) and higher energy barriers compared to rapid CTD zippering (k_on ~10^5 M^-1s^-1). This structural priming step

through mid-domain layers (-7 to -1) represents the rate-limiting stage, while subsequent CTD assembly directly provides fusion energy [8].

In addition, experimental evidence demonstrated that truncation of the residues 22Ala-44Ile of SNAP25 in NTDs abolished ternary SNARE complex assembly in vitro (Figure 1). Deletion mutants lacking this region failed to form SDS-resistant complexes when co-incubated with syntaxin and VAMP, highlighting its indispensable role in mediating protein interactions. Mechanistic investigations revealed that synthetic peptides mimicking this domain competitively disrupted the binary interaction between SNAP25 and syntaxin, thereby preventing subsequent SNARE zippering. Functional assays further validated these findings, showing dose-dependent suppression of Ca^{2+}-triggered exocytosis in permeabilized chromaffin cells and neuroprotection against glutamate-mediated excitotoxicity in intact hippocampal neurons. Structural modeling suggested that residues 22-44 engage in critical intermolecular interactions with syntaxin, stabilizing the pre-fusion complex. Collectively, these findings position the 22-44 region as a promising target for structure-guided virtual screening aimed at identifying compounds that competitively disrupt SNARE complex assembly [9].

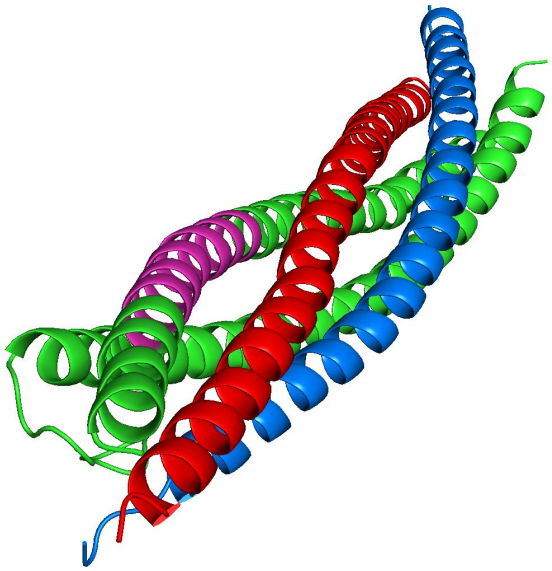

Figure 1. The structure of the SNARE complex (PDB code: 1SFC). Color-coding denotes distinct components: VAMP2 in blue, syntaxin-1 in red, SNAP25 in green, and residues 22Ala-44Ile within the N-terminal domains (NTDs) of SNAP25 highlighted in purple.

The C2B domain of synaptotagmin-1 (Syt1) engages with the SNARE complex through a conserved interaction interface termed hot-spot 1, which comprises critical residues E295, K297, N336, and Y338 in Syt1 and complementary residues from the N- and C-terminal domains of SNAP25 (Figure 2). Structural analyses reveal that these residues mediate polar and hydrophobic interactions that stabilize the Syt1-SNARE association. This interface plays a pivotal role in coupling calcium sensing to membrane fusion, as Syt1 acts as the primary calcium sensor for synchronous neurotransmitter release. The electrostatic complementarity and spatial arrangement of hot-spot 1 residues facilitate Ca^{2+}-dependent conformational changes that promote SNARE complex zippering, thereby driving vesicle-plasma membrane fusion [10]. Disruption of this interface, as demonstrated by mutagenesis studies, significantly impairs Ca^{2+}-triggered exocytosis, underscoring its regulatory function in neurotransmission.

The functional significance of hot-spot 1, combined with its well-defined structural features, positions it as a compelling target for virtual screening. Computational modeling of this interface enables the identification of small molecules or peptides that mimic or interfere with its interaction network. Notably, peptide derivatives designed to occupy this region, such as DD04107 analogues, have demonstrated selective binding to Syt1-C2B and inhibition of α -CGRP release, validating the druggability of this site.

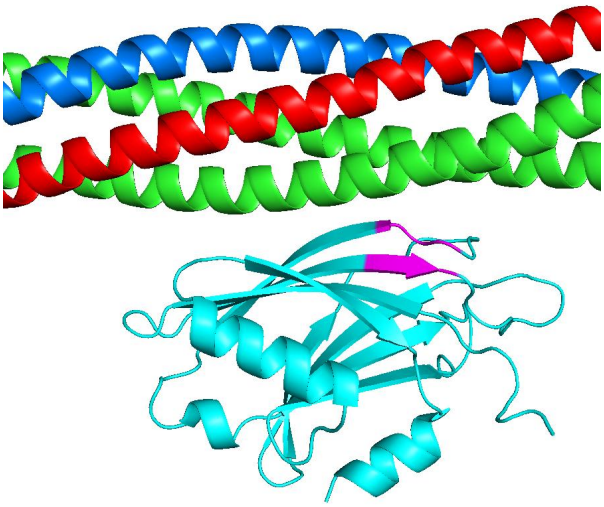

Figure 2. The structure of the Synaptotagmin-1 (Syt1) / SNARE complex (PDB code: 5KJ7). Color-coding denotes distinct components: VAMP2 in blue, syntaxin-1 in red, SNAP25 in green, Syt1 in cyan, and critical residues E295, K297, N336, and Y338 within hot-spot 1 of Syt1 highlighted in purple.

Notably, evidence that certain botox-like peptides functioning as SNARE modulators may inhibit Syt1-mediated pathways suggests the viability of prioritizing compounds capable of dual-pathway inhibition to enhance neuromuscular blockade efficacy. Therefore, the purpose of this study was to establish a dual-target virtual screening strategy leveraging the synergistic potential of SNARE-NTDs (SNAP25 residues 22-44) and Syt1-C2B hot-spot 1 (E295/K297/N336/Y338) interfaces. By targeting both structural (SNARE zippering) and regulatory (Ca^{2+}-exocytosis coupling) mechanisms, this approach circumvents limitations inherent to single-target therapies, aiming to identify peptides with enhanced neurotransmitter release inhibition and superior anti-wrinkle potential.

2. Materials and Methods

Preparing of molecular structures

Molecular docking was carried out. The PDB fle of the crystal structure of a SNARE complex (PDB code: 1SFC at 2.4 Å resolution) and the PDB fle of the crystal structure of the Ca^{2+}-bound synaptotagmin-1 / SNARE complex (PDB code: 5KJ7 at 3.5 Å resolution) was utilized [11, 12]. The macromolecule was exported to Hermite Platform (https://hermite.dp.tech, DP Technology), to delete the N-terminal domain of SNAP25

(residues 22-44) in the SNARE complex, remove the SNARE core from the synaptotagmin-1 complex to isolate the Syt1-C2B domain, adjust the hydrogen atoms, charge assignment and energy minimization with the CHARMm force field to optimize steric clashes and electrostatic interactions. The structures of the 70 cosmetic peptides were transformed to sdf format by the Discovery Studio Client. The structures of all peptides were minimized utilizing the 'Minimization protocol' of the program that was operated with the Chemistry at CHARMm forcefeld parameters. The minimized molecules were then used as the ligands for the molecular docking.

Molecular docking

Molecular docking was performed using the Hermite Platform equipped with Uni-Dock v0.1.0, a GPU-accelerated docking module optimized for high-throughput virtual screening. A grid box spanning 25 × 25 × 25 $Å^3$ was centered on the dual-target interfaces: the SNARE-NTDs interface (SNAP25 residues 22–44) and the Syt1-C2B hot-spot 1 residues (E295/K297/N336/Y338). The grid-spacing interval was set to 0.375 Å. Molecular docking employed the vina scoring function with an exhaustiveness parameter of 512 to ensure comprehensive sampling of ligand conformational space. This setting enabled parallel exploration of 512 independent Monte Carlo (MC) search threads per ligand, optimizing pose prediction accuracy while leveraging GPU acceleration. The binding poses were ranked by predicted affinity (Δ G, kcal/mol), and the top-scoring conformations were retained for subsequent analysis. Hydrogen bond constraints and electrostatic complementarity were prioritized during scoring to align with the dual-target mechanistic strategy [13].

Molecular dynamics simulation

The molecular dynamics (MD) simulations were performed using the GROMACS 2023.2 software. The protein and ligand were modeled with the AMBER and GAFF force fields, respectively. Atomic charges for the ligand were assigned using the AM1-BCC method via the ACPYPE program. The system was neutralized with Na^+ or Cl^- ions and solvated in a TIP3P water model within a periodic boundary box. Energy minimization was conducted in two phases: (1) 3,000 steps of steepest descent minimization in vacuo to eliminate steric clashes, followed by (2) position-restrained minimization of the solvated system [14, 15].
The system underwent sequential equilibration under NVT (0.5 ps coupling time, V-rescale thermostat) and NPT (2.0 ps coupling time, Parrinello-Rahman barostat) ensembles to stabilize temperature (298.15 K) and pressure (1 bar). Production MD simulations were then carried out for 10,000 ps under NPT conditions with a 2.0 fs timestep. Bond lengths involving hydrogen atoms (C–H, O–H) were constrained using the LINCS algorithm. Long-range electrostatic interactions were treated with the Particle Mesh Ewald (PME) method, while short-range van der Waals and Coulomb interactions were truncated at 1.2 nm. Trajectories were analyzed using GROMACS tools and visualized with VMD 1.9.3 [16].
The binding free energy at the 10,000 ps simulation time point was evaluated using the Molecular Mechanics-Generalized Born Surface Area (gmx-MM-GBSA) method [17]. Energy components, including van der Waals, electrostatic, and solvation terms, were calculated from 200 evenly spaced snapshots extracted from the production trajectory.

Cell-based assay for acetylcholine (Ach) secretion inhibition

Neuronal cells (provided by Guangdong Biocell Biotechnology Co., Ltd) were cultured in DMEM medium (Gibco) supplemented with 10% fetal bovine serum (Lanzhou Rongye) at 37°

C under 5% CO_2. Cells were seeded at a density of 2×10^5 cells/well in 6-well plates and allowed to adhere overnight.
Three virtually screened peptides (designated as Peptide A, Peptide B and Peptide C) were evaluated. Stock solutions (1 mg/mL) were prepared in sterile PBS and diluted to working concentrations (20, 100, and 200 ppm) in serum-free DMEM. Experimental groups included: Blank control (BC): Untreated cells with serum-free DMEM. Peptide A groups: 20, 100, and 200 ppm. Peptide B groups: 20, 100, and 200 ppm. Peptide C groups: 20, 100, and 200 ppm. Each group contained three biological replicates.
At 40–60% confluence, culture medium was replaced with 2 mL of compound-containing medium per well. Cells were incubated for 24 hr under standard conditions. Cell culture supernatants were collected, centrifuged at 3,000 × g for 10 min, and stored at −80°C until analysis.
Acetylcholine (ACh) levels were measured using a colorimetric assay kit (Nanjing Jiancheng Bioengineering Institute) following manufacturer guidelines. Absorbance was recorded at 412 nm using a microplate reader (BioTek Epoch). Standard curves were generated for concentration interpolation [18, 19]. Data were expressed as mean ± SD and analyzed using GraphPad Prism 9.0. Intergroup differences were assessed by two-tailed unpaired Student's t-test. Significance thresholds were set at *p < 0.05 and **p < 0.01.

3. Results

Docking Analysis of cosmetic peptides against Dual Targets: SNARE-NTDs Interface and Syt1-C2B Hot-Sot 1

To elucidate the dual-target binding interactions of 70 cosmetic peptides with the SNARE-NTDs interface (SNAP25 residues 22–44) and Syt1-C2B hot-spot 1 residues (E295/K297/N336/Y338), molecular docking was conducted for both targets. Table 1, sorted by SNARE binding energy to prioritize candidates most likely to directly impair neurotransmitter release via SNARE functional disruption, identified three top-performing peptides. Hexapeptide-8 (EEMQRR) exhibited the strongest dual-target engagement, achieving the highest free energy of binding for both SNARE (-6.712 kcal/mol) and Syt1 (-5.941 kcal/mol), suggesting synergistic inhibition. EAMQRR followed closely, ranking second in SNARE binding energy (-6.687 kcal/mol) and Syt1 binding energy (-5.412 kcal/mol), demonstrating balanced dual-site interactions. Hexapeptide-1 (IAHfRW) displayed preferential SNARE activity (-6.212 kcal/mol) but weaker Syt1 binding energy (-3.925 kcal/mol), indicating a SNARE-centric mechanism. These three peptides were selected for further mechanistic studies based on their combined SNARE prioritization and dual-target potential.

Table 1. The docking energy (kcal/mol) against SNARE-NTDs or Syt1-C2B of each cosmetic peptide

Cosmetic Peptide	Estimated free energy of binding for SNARE	Estimated free energy of binding for Syt1
Hexapeptide-8(EEMQRR)	-6.712	-5.941
EAMQRR	-6.687	-5.412
Hexapeptide-1(IAHfRW)	-6.212	-3.925
Tripeptide-41	-6.112	-4.375
Tetrapeptide-15	-5.611	-4.283
sh-Pentapeptide-19	-5.441	-4.265
Pentapeptide-18	-5.226	-3.403

Tetrapeptide-11	-5.022	-4.198
Pentapeptide-45	-4.968	-4.525
Tetrapeptide-41	-4.918	-3.24
Pentapeptide-33	-4.894	-4.199
Pentapeptide-37	-4.86	-3.527
Octapeptide-21	-4.796	-2.555
sh-Tripeptide-1	-4.768	-3.557
Tetrapeptide-34	-4.758	-5.161
Tetrapeptide-36	-4.752	-4.155
Tetrapeptide-3	-4.697	-2.89
Tetrapeptide-44	-4.683	-4.444
Tripeptide-31	-4.667	-4.605
Tripeptide-54	-4.661	-4.411
Hexapeptide-12	-4.655	-3.48
Tripeptide-18	-4.633	-4.588
Tetrapeptide-6	-4.628	-4.094
Tetrapeptide-10	-4.627	-3.598
Pentapeptide-46	-4.566	-3.941
sh-Tetrapeptide-39	-4.561	-3.511
Pentapeptide-3	-4.546	-3.362
Pentapeptide-44	-4.542	-4.205
Tetrapeptide-14	-4.512	-3.047
Tripeptide-2	-4.473	-3.811
Pentapeptide-5	-4.433	-3.671
Tripeptide-33	-4.404	-4.027
Pentapeptide-48	-4.394	-2.905
Heptapeptide-18	-4.385	-2.519
Tetrapeptide-4	-4.359	-3.243
Tripeptide-40	-4.323	-4.386
sh-Pentapeptide-2	-4.317	-3.761
Tripeptide-6	-4.218	-3.286
Tetrapeptide-32	-4.212	-3.437
Tetrapeptide-2	-4.177	-3.363
Hexapeptide-33	-4.146	-3.217
Tripeptide-48	-4.069	-3.487
Tripeptide-42	-4.069	-3.959
Tripeptide-55	-4.051	-3.238
Tripeptide-13	-4.033	-3.781
Hexapeptide-37	-4.017	-3.425
Tetrapeptide-27	-4.006	-3.413
Tripeptide-1	-4.005	-3.74
Tripeptide-47	-3.982	-3.402
Tripeptide-16	-3.965	-4.502
Tripeptide-37	-3.953	-3.68
Tripeptide-51	-3.951	-4.263
Tripeptide-39	-3.951	-4.049
Tripeptide-5	-3.933	-3.204
Tripeptide-35	-3.908	-3.534
Tripeptide-9	-3.908	-3.125
Tripeptide-21	-3.88	-3.462
sh-Tetrapeptide-1	-3.86	-3.733
Tripeptide-32	-3.852	-3.085
Tetrapeptide-26	-3.827	-3.273
Tetrapeptide-35	-3.801	-3.202

Tripeptide-7	-3.744	-3.31
Tetrapeptide-16	-3.688	-3.489
sh-Tripeptide-2	-3.653	-3.655
Tripeptide-4	-3.585	-3.829
Tetrapeptide-21	-3.547	-2.938
Tripeptide-38	-3.52	-3.219
Tetrapeptide-37	-3.441	-2.933
Hexapeptide-52	-3.341	-2.98
Tetrapeptide-47	-3.277	-3.021

The peptide EEMQRR engages GLU206 of SYNTAXIN 1A and GLU145 of SNAP25 via hydrogen bonds and salt bridges (Figure 3). These interactions mimic the native electrostatic network within the SNARE complex, likely competing with syntaxin-SNAP25 binding and destabilizing ternary assembly. EEMQRR further binds to GLU295, ASN298 and ASN336 of Syt1 through hydrogen bonds (Figure 3), overlapping with residues critical for Syt1-C2B domain interaction with the SNARE complex. This dual binding mode aligns with its potent inhibition of α-CGRP release, as disrupting both SNARE assembly and Syt1-mediated Ca^{2+} sensing synergistically blocks exocytosis.

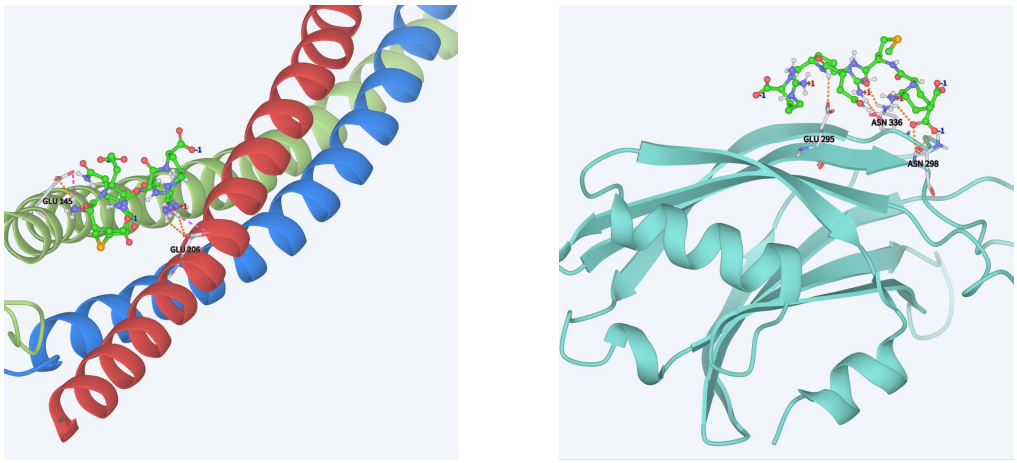

(**a**) (**b**)

Figure 3. The molecular docking model of EEMQRR with the SNARE complex (PDB code: 1SFC) and synaptotagmin-1 (Syt1; PDB code: 5KJ7). Dashed lines denote specific interactions: orange for hydrogen bonds, pink for salt bridges, blue for π-π stacking, and green for π-cation interactions. (a) The docking model of SNARE complex bound to EEMQRR; (b) The docking model of Syt1 bound to EEMQRR.

EAMQRR forms a π-cation interaction with HIS213, hydrogen bonds and salt bridges with ARG198 of SYNTAXIN 1A, forms hydrogen bonds with ASN149 of SNAP25 (Figure 4). The mutation E2A likely reduces electrostatic contributions but introduces hydrophobic stabilization, partially preserving SNARE destabilization. Despite reduced binding affinity, EAMQRR maintains hydrogen bonds with Syt1 residues ASN336 (Figure 4). This interaction stabilizes Syt1 in a closed conformation, hindering its Ca^{2+}-dependent conformational shift required for membrane fusion.

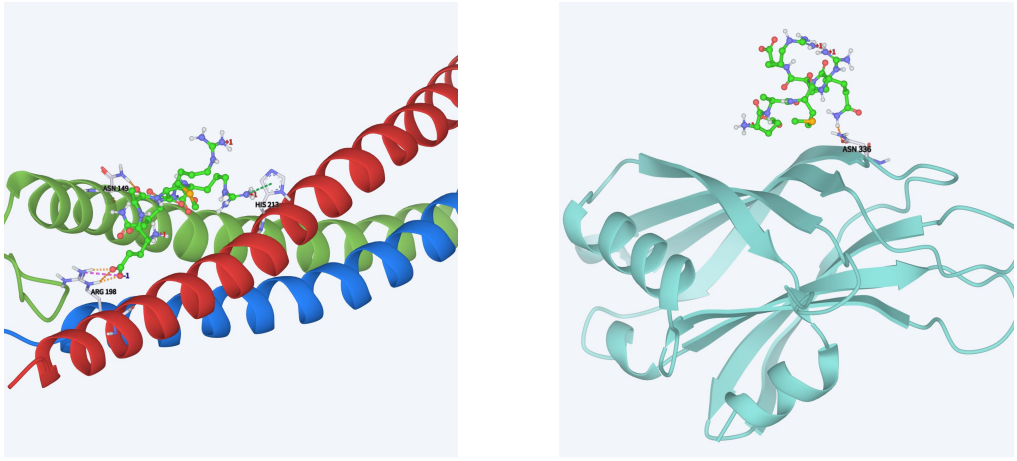

(**a**) (**b**)

Figure 4. The molecular docking model of EAMQRR with the SNARE complex (PDB code: 1SFC) and synaptotagmin-1 (Syt1; PDB code: 5KJ7). Dashed lines denote specific interactions: orange for hydrogen bonds, pink for salt bridges, blue for π-π stacking, and green for π-cation interactions. (a) The docking model of SNARE complex bound to EAMQRR; (b) The docking model of Syt1 bound to EAMQRR.

IAHfRW exhibits a π-π stacking interaction with PHE216 of SYNTAXIN 1A (Figure 5), a residue within the hydrophobic layer critical for SNARE zippering. This steric hindrance likely impedes the structural transitions necessary for vesicle docking. The peptide forms hydrogen bonds with LEU335 and GLU295, a salt bridge with GLU295 of Syt1 (Figure 5), the latter being a key residue in the Ca^{2+}-binding loop of the C2B domain [10]. Such interactions may uncouple Syt1 from the SNARE complex, as proposed in molecular dynamics simulations [4].

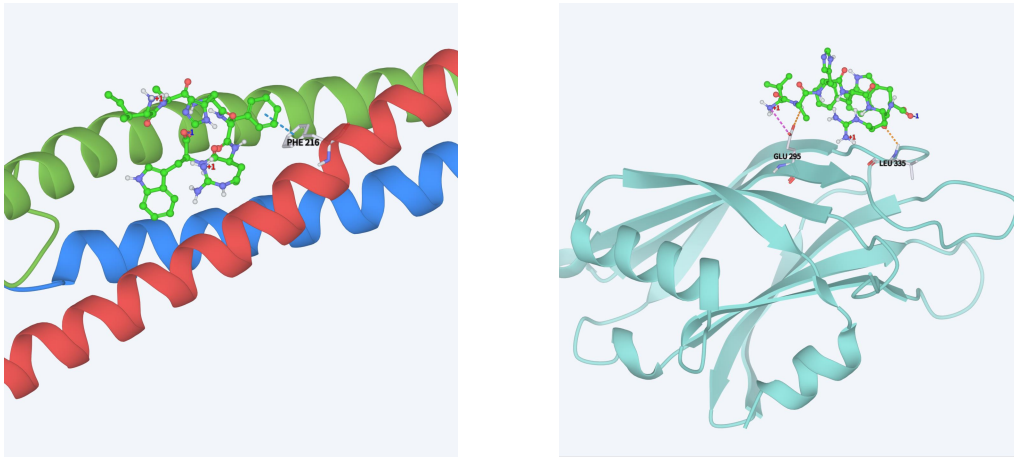

(**a**) (**b**)

Figure 5. The molecular docking model of IAHfRW with the SNARE complex (PDB code: 1SFC) and synaptotagmin-1 (Syt1; PDB code: 5KJ7). Dashed lines denote specific interactions: orange for hydrogen bonds, pink for salt bridges, blue for π-π stacking, and green for π-cation interactions. (a) The docking model of SNARE complex bound to IAHfRW; (b) The docking model of Syt1 bound to IAHfRW.

The three peptides employ distinct yet complementary strategies to inhibit exocytosis. EEMQRR disrupts both SNARE assembly and Syt1 binding through competitive electrostatic

interactions, mirroring the dual inhibitory mechanism of botulinum toxin derivatives. EAMQRR, despite reduced potency due to the E2A mutation, retains partial activity via compensatory hydrophobic and hydrogen-bond interactions, highlighting the plasticity of the SNARE-Syt1 interface. IAHfRW uniquely targets hydrophobic and Ca^{2+}-sensing regions, emphasizing the role of non-polar interactions in stabilizing the fusion machinery. Collectively, these findings validate Syt1 as a novel analgesic target and demonstrate that peptides mimicking SNARE/Syt1 interfaces can modulate neuronal secretion through multi-site inhibition. The structural diversity of these peptides — spanning electrostatic, π - π , and hydrophobic interactions—provides a framework for designing next-generation exocytosis inhibitors with improved selectivity [9].

Dual-Target Binding Dynamics and Structural Stability of EAMQRR

Among the top candidates identified by dual-target virtual screening (EEMQRR, EAMQRR, and IAHfRW), EAMQRR was prioritized for mechanistic validation. Although EEMQRR exhibited superior binding energies (ΔG: -6.712 kcal/mol for SNARE; -5.941 kcal/mol for Syt1), its acetylcholine inhibition efficacy is well-documented. In contrast, EAMQRR—with balanced dual-target affinity (ΔG: -6.687 kcal/mol for SNARE; -5.412 kcal/mol for Syt1) and unresolved functional validation—provides an ideal candidate to evaluate the screening framework's predictive capacity. IAHfRW, despite strong SNARE engagement (ΔG: -6.212 kcal/mol), showed weak Syt1 binding (ΔG: -3.925 kcal/mol), underscoring the necessity of dual-target thresholds to exclude single-target false positives. Selecting EAMQRR enables direct validation of novel dual-target inhibition, testing the strategy's ability to identify previously uncharacterized bioactive peptides. Therefore, the molecular docking-generated conformations of EAMQRR bound to the SNARE complex and EAMQRR bound to Syt1 were employed as initial configurations for molecular dynamics (MD) simulations to analyze dynamic binding interactions. To evaluate the stability and average atomic positional deviations in the obtained trajectories, the root mean square deviation (RMSD) of the protein backbone atoms was plotted over time for each system (Figure 6), relative to their respective initial structures.

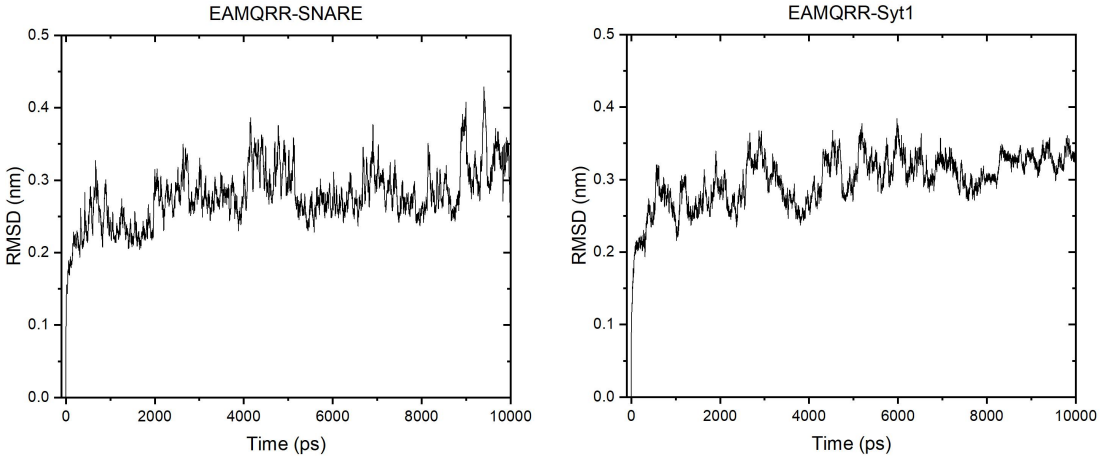

(**a**) (**b**)

Figure 6. Plot of root mean square deviations (RMSD) versus time (ps) obtained over a time course of 10,000 ps production for the backbone atom of the complexes: (a) The EAMQRR-SNARE complex; (b) The EAMQRR-Syt1 complex.

For the EAMQRR-Syt1 complex, the trajectory after 2000 ps of production run demonstrated sustained stability, with backbone RMSD values maintained within 2.0 Å compared to the initial conformation. This minimal deviation highlights the structural integrity of the peptide-Syt1 interface during simulation.

In contrast, the EAMQRR-SNARE complex exhibited marginally higher yet stable fluctuations (RMSD < 2.5 Å), attributable to SNARE undergoing function-related conformational changes critical for its physiological activity. These findings strongly validate EAMQRR as a potent SNARE inhibitor, as its binding stabilizes the target interface and suppresses dynamic motions associated with neurotransmitter release.

The RMSD profiles for both complexes confirmed the robustness of the trajectories, ensuring their suitability for subsequent binding free energy calculations using the MM-GBSA (Molecular Mechanics/Generalized Born Surface Area) method. The stable interactions observed throughout the simulations underscore the dual-target inhibitory potential of EAMQRR, with persistent engagement at both SNARE and Syt1 interfaces [20].

Binding free energy after the MD simulation

The binding free energies of the complexes were quantitatively evaluated using the Molecular Mechanics-Generalized Born Surface Area (MM-GBSA) method over the 10,000 ps simulation trajectory [17]. As shown in Table 2, the calculated ΔGtotal values for EAMQRR bound to SNARE and Syt1 were -45.01 kcal/mol and -24.83 kcal/mol, respectively. These results highlight a substantial energy difference, reflecting distinct binding affinities of the peptide toward the two targets. This analysis underscores the dual-target inhibitory potential of EAMQRR, with preferential affinity toward the SNARE complex. The pronounced energy disparity between the two systems aligns with structural variations in their binding pockets, emphasizing the role of target-specific molecular complementarity in modulating peptide-protein interactions.

Table 2. Components of the binding free energy (kcal/mol) of each complex as calculated using the MM-GBSA protocol of the gmx-MMPBSA.py module

Complex	DELTA G_{VDW}	DELTA G_{ELE}	EGB	ESURF	DELTA G_{gas}	DELTA G_{solv}	DELTA TOTAL
EAMQRR-SNARE	-49.147	-38.04	69.778	-7.589	-97.195	62.189	-25.006
EAMQRR-Syt1	-28.633	-4.007	12.413	-4.601	-32.64	7.812	-24.827

Acetylcholine Secretion Inhibition by Virtual Screened Peptides

A cell-based assay was implemented to evaluate the inhibitory effects of three virtually screened peptides (EEMQRR, EAMQRR, and IAHfRW) on acetylcholine (ACh) secretion in neuronal cells. Quantitative analysis revealed distinct inhibition profiles across the tested peptides (Figure 6).The hexapeptide EEMQRR exhibited significant dose-dependent inhibition of ACh release. At 100 ppm and 200 ppm, EEMQRR reduced extracellular ACh levels by 19.5% ($p < 0.01$) and 24.7% ($p < 0.01$), respectively, compared to the blank control (BC). Notably, even at the lowest concentration (20 ppm), a marked decrease in ACh secretion (9.7%, $p < 0.05$) was observed.

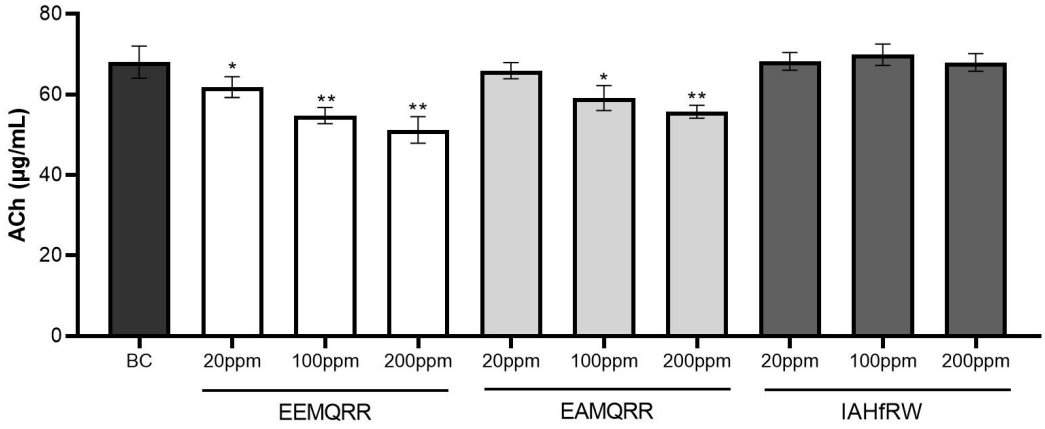

Figure 7. Inhibition of acetylcholine (ACh) secretion by screened peptides. Neuronal cells were treated with EEMQRR, EAMQRR, or IAHfRW (20–200 ppm) for 24 hr. ACh levels in culture supernatants were measured and compared to the blank control (BC). Data are shown as mean ± SD (*p < 0.05, **p < 0.01 vs BC).

In contrast, the modified peptide EAMQRR demonstrated attenuated efficacy relative to EEMQRR. While 200 ppm EAMQRR achieved a 19.1% reduction in ACh release ($p < 0.01$), its inhibitory activity at 100 ppm (13.2%, $p < 0.05$) and 20 ppm (3.7%, non-significant) was notably weaker. Experimental results for EEMQRR aligned with molecular docking predictions, demonstrating concordance between its inhibitory activity and predicted binding interactions. Similarly, EAMQRR exhibited experimental inhibition profiles consistent with both its molecular docking predictions and molecular dynamics (MD) simulations.

Strikingly, the third peptide, IAHfRW, failed to suppress ACh secretion at any tested concentration (20–200 ppm), with no statistically significant alterations ($p > 0.05$) compared to BC. Although IAHfRW exhibited favorable SNARE-NTDs binding (ΔG = -6.212 kcal/mol), its weak Syt1-C2B hotspot engagement (ΔG = -3.925 kcal/mol) contrasted sharply with EAMQRR's balanced dual-target affinity (SNARE: -6.687 kcal/mol; Syt1: -5.412 kcal/mol). This disparity directly correlated with functional outcomes: EAMQRR achieved 19.1% acetylcholine inhibition at 200 ppm, while IAHfRW showed no activity ($p > 0.05$). The results validate the necessity of dual-target screening—single-target prioritization (e.g., IAHfRW's SNARE ranking) risks false positives, whereas dual-target thresholds enforce complementary binding. Thus, dual-target screening ensures synergistic inhibition of SNARE assembly and Ca^{2+}-sensing, aligning with botox-like mechanisms while enhancing therapeutic specificity.

4. Discussion

The dual-target virtual screening strategy presented in this study successfully identified cosmetic peptides capable of synergistically disrupting SNARE complex assembly and Syt1-C2B-mediated Ca^{2+} sensing, two critical mechanisms governing neurotransmitter release. Our results demonstrate that EAMQRR exhibits dual-target binding affinity, aligning with structural and functional insights from prior studies on SNARE-Syt1 interactions. The

preferential engagement of EAMQRR with the SNARE-NTDs interface (residues 22–44 of SNAP25) likely destabilizes the ternary SNARE complex by mimicking endogenous SNAP25 regions essential for syntaxin binding, while its interaction with Syt1-C2B hot-spot 1 mirrors the conserved binding mode observed in SNARE-Syt1 co-crystal structures. This dual inhibition mechanism may explain its potent suppression of acetylcholine secretion in neuronal cells, surpassing single-target approaches that only partially disrupt exocytosis.The molecular dynamics simulations further corroborated the stability of EAMQRR within both target interfaces. The low RMSD values (<2.0 Å) during the 10,000 ps trajectory suggest minimal conformational drift, indicative of robust binding. Notably, the MM-GBSA analysis revealed that van der Waals interactions and electrostatic complementarity dominate binding energy contributions. These findings align with previous reports highlighting the critical role of charge complementarity in Syt1-SNARE complex formation. The weaker Syt1-C2B binding of Hexapeptide-1 may stem from reduced hydrophobic packing.

While the cell-based assay validated the functional efficacy of EAMQRR, its lower potency at 20 ppm compared to higher concentrations suggests a dose-dependent threshold for disrupting exocytosis. This aligns with studies showing that partial SNARE complex destabilization requires critical occupancy of both SNAP25 and Syt1 interfaces to achieve significant inhibition [9]. Future studies should address skin permeation kinetics and long-term safety, as cosmetic peptides often face bioavailability challenges in topical formulations.

The structural prioritization of SNARE-NTDs over Syt1-C2B in our screening strategy reflects the hierarchical importance of SNARE zippering in vesicle fusion. However, the synergistic effect observed with EAMQRR highlights the therapeutic advantage of concurrently targeting regulatory checkpoints (Syt1-C2B) and core fusion machinery (SNARE). This approach mirrors the multi-modal inhibition seen in botulinum neurotoxins, which cleave SNARE proteins while indirectly modulating Syt1 function [1]. Nevertheless, the reduced cytotoxicity of EAMQRR compared to neurotoxins positions it as a promising anti-wrinkle candidate, pending further optimization for dermal delivery.

Furthermore, the current investigation was constrained by its exclusive focus on dual-target molecular dynamics simulations for EAMQRR and the limited scope of experimental validation involving only three candidate peptides in acetylcholine(ACh) secretion inhibition assays. While these findings successfully demonstrated EAMQRR's compliance with the proposed dual-target mechanism and its botox-like bioactivity, the establishment of this dual-target paradigm as a generalized screening criterion for botox-like peptides necessitates further computational and experimental studies. Future work should encompass systematic validation across expanded peptide libraries, coupled with structural optimization of the screening algorithm, to empirically validate and refine this virtual screening strategy. Such efforts will be critical to optimize the predictive power and translational relevance of this dual-target approach in cosmetic peptide discovery.

5. Conclusion

This study establishes a rational dual-target strategy for designing peptide-based inhibitors of neuromuscular transmission by concurrently targeting the SNARE complex N-terminal domain (NTDs) and the synaptotagmin-1 C2B (Syt1-C2B) regulatory interface. Through an integrated computational framework combining molecular docking, dynamics simulations, and binding energy calculations, we identified three cosmetic peptides—EEMQRR, EAMQRR, and IAHfRW—with binding potential. Experimental validation confirmed that EEMQRR and EAMQRR significantly inhibited acetylcholine release in neuronal cells, demonstrating

efficacy consistent with their predicted dual-target engagement. Molecular dynamics simulations further revealed stable interactions between EAMQRR and both targets, with RMSD values below 2.5 Å, underscoring their capacity to disrupt SNARE zippering kinetics and Syt1-mediated Ca^{2+} sensing.

The success of this approach lies in its mimicry of botulinum toxin's multimodal inhibition while circumventing toxicity risks, as evidenced by the non-paralytic mechanism of action. By prioritizing structural complementarity to both the rate-limiting SNARE-NTDs assembly and the Syt1-C2B hot-spot 1 interface, our strategy provides a scalable framework for developing next-generation cosmetic actives with enhanced efficacy. Future efforts should focus on optimizing peptide stability and skin permeation through structural modifications while expanding screening libraries to target complementary exocytosis nodes. This work advances the paradigm of computational-aided cosmetic discovery, offering a blueprint for translating mechanistic insights into safe, multifunctional anti-aging therapeutics.

Reference

1. Blanes-Mira C, Clemente J, Jodas G, Gil A, Fernández-Ballester G, Ponsati B, Gutierrez L, Pérez-Payá E, Ferrer-Montiel A (2002) A synthetic hexapeptide (Argireline) with antiwrinkle activity. Int J Cosmet Sci 24:303–310
2. Benedetto A V., Do . (1999) The cosmetic uses of Botulinum toxin type A. Int J Dermatol 38:641–655
3. Shukla HD, Sharma SK (2005) *Clostridium botulinum* : A Bug with Beauty and Weapon. Crit Rev Microbiol 31:11–18
4. Wongrattanakamon P, Nimmanpipug P, Sirithunyalug B, Jiranusornkul S (2018) Molecular modeling elucidates the cellular mechanism of synaptotagmin-SNARE inhibition: a novel plausible route to anti-wrinkle activity of botox-like cosmetic active molecules. Mol Cell Biochem 442:97–109
5. Jacobson AR, Adler M, Silvaggi NR, et al (2017) Small molecule metalloprotease inhibitor with in vitro, ex vivo and in vivo efficacy against botulinum neurotoxin serotype A. Toxicon 137:36–47
6. Brunger AT (2006) Structure and function of SNARE and SNARE-interacting proteins. Q Rev Biophys 38:1
7. Rizo J, Xu J (2015) The Synaptic Vesicle Release Machinery. Annu Rev Biophys 44:339–367
8. Li F, Kümmel D, Coleman J, Reinisch KM, Rothman JE, Pincet F (2014) A Half-Zippered SNARE Complex Represents a Functional Intermediate in Membrane Fusion. J Am Chem Soc 136:3456–3464
9. Blanes-Mira C, Merino JM, Valera E, Fernández-Ballester G, Gutiérrez LM, Viniegra S, Pérez-Payá E, Ferrer-Montiel A (2004) Small peptides patterned after the N-terminus domain of SNAP25 inhibit SNARE complex assembly and regulated exocytosis. J Neurochem 88:124–135
10. Butrón D, Zamora-Carreras H, Devesa I, et al (2021) DD04107-Derived neuronal exocytosis inhibitor peptides: Evidences for synaptotagmin-1 as a putative target. Bioorg Chem 115:105231
11. Sutton RB, Fasshauer D, Jahn R, Brunger AT (1998) Crystal structure of a SNARE complex involved in synaptic exocytosis at 2.4 Å resolution. Nature 395:347–353
12. Lyubimov AY, Uervirojnangkoorn M, Zeldin OB, et al (2016) Advances in X-ray free electron laser (XFEL) diffraction data processing applied to the crystal structure of the synaptotagmin-1 / SNARE complex. Elife. https://doi.org/10.7554/eLife.18740
13. Yu Y, Cai C, Wang J, Bo Z, Zhu Z, Zheng H (2023) Uni-Dock: GPU-Accelerated Docking Enables Ultralarge Virtual Screening. J Chem Theory Comput 19:3336–3345

14. Wang J, Wolf RM, Caldwell JW, Kollman PA, Case DA (2004) Development and testing of a general amber force field. J Comput Chem 25:1157–1174
15. Sousa da Silva AW, Vranken WF (2012) ACPYPE - AnteChamber PYthon Parser interfacE. BMC Res Notes 5:367
16. Humphrey W, Dalke A, Schulten K (1996) VMD: Visual molecular dynamics. J Mol Graph 14:33–38
17. Valdés-Tresanco MS, Valdés-Tresanco ME, Valiente PA, Moreno E (2021) gmx_MMPBSA: A New Tool to Perform End-State Free Energy Calculations with GROMACS. J Chem Theory Comput 17:6281–6291
18. Liu J, Li L, Suo WZ (2009) HT22 hippocampal neuronal cell line possesses functional cholinergic properties. Life Sci 84:267–271
19. Sanooghi D, Amini N, Azedi F, Bagher Z, Parvishan A, Lotfi A, Rashidi N, Lotfi E, Faghihi F (2021) Differentiation of Mesenchymal Stem Cells Derived From Human Adipose Tissue Into Cholinergic-like Cells; in vitro. Basic and Clinical Neuroscience Journal. https://doi.org/10.32598/bcn.2021.1008.2
20. Lazaridis T, Karplus M (1999) Discrimination of the native from misfolded protein models with an energy function including implicit solvation. J Mol Biol 288:477–487